Environmental and Experimental Botany 229 (2025) 106044

Contents lists available at ScienceDirect

Environmental and Experimental Botany

journal homepage: www.elsevier.com/locate/envexpbot

Research paper

Light-nutrient interaction orchestrates leaf dynamics, nitrogen assimilation, and cellular energetics in *Agastache rugosa* (Fisch. & C.A.Mey.) Kuntze

Khairul Azree Rosli [a,*], Azizah Misran [a], Latifah Saiful Yazan [b], Puteri Edaroyati Megat Wahab [a]

[a] Department of Crop Science, Faculty of Agriculture, Universiti Putra Malaysia, 43400 UPM Serdang, Selangor, Malaysia
[b] Department of Biomedical Sciences, Faculty of Medicine and Health Sciences, Universiti Putra Malaysia, 43400 UPM Serdang, Selangor, Malaysia

ARTICLE INFO

Keywords:
Agastache rugosa
Light, nutrient
Leaf dynamics
Nitrogen
Proton pump

ABSTRACT

Light and nutrients are vital environmental factors shaping plant growth and metabolism, yet their interactive effects on leaf dynamics, nitrogen assimilation, and cellular energetics remain largely unexplored. We aimed to investigate these processes in *Agastache rugosa* (Fisch. & C.A.Mey.) Kuntze under two light levels; high-light (HL, 0 % shade) and low-light (LL, 50 % shade) combined with four nutrient levels; low (NPK1, 40 mg kg^{-1}), moderate (NPK2, 80 mg kg^{-1}), high (NPK3, 120 mg kg^{-1}) and very high (NPK4, 160 mg kg^{-1}). High-light conditions and high-nutrient levels (HL-NPK3) synergistically enhanced leaf mass area by 44 % with net photosynthesis rates and nitrate reductase activity increasing by up to 17.62 ± 0.89 μmol CO_2 m^{-2} s^{-1} and 0.34 ± 0.02 μmol NO_2 cm^{-2} h^{-1} each. Low-light and moderate-nutrient levels (LL-NPK2) triggered a 42 % increase in specific leaf area and threefold higher photosynthetic nitrogen use efficiency. Unexpectedly, high-light and moderate-nutrient levels (HL-NPK2) elicited peak vacuolar H^+-ATPase and H^+-pyrophosphatase activities at 15.6 % and 53.1 % each. This study also found significant positive correlations between chlorophyll content, nitrate reductase ($r = 0.62$, $P < 0.01$), and vacuolar H^+-ATPase activity ($r = 0.58$, $P < 0.01$), suggesting a mechanism for maintaining high photosynthetic capacity and efficient nitrogen assimilation. The clustering of leaf area index, specific leaf area, and photosynthetic nitrogen use efficiency (similarity of > 70 %) suggests optimized leaf structure and nitrogen use in light-limited but nutrient-rich environments. Our findings show how *A. rugosa* adjusts its physiology in response to environmental conditions, with implications for understanding plant adaptation and improving cultivation practices.

1. Introduction

Plants exhibit remarkable plasticity in response to environmental factors, with light and nutrient availability being two of the most critical determinants of growth, development, and physiological processes (Arnold et al., 2019). These environmental cues affect a wide array of plant traits, from leaf structure and photosynthetic capacity to nitrogen metabolism and the distribution of resources (Hikosaka et al., 2014). Besides its putative role in photosynthesis, light signaling regulates nutrient uptake and assimilation in plants via specific transcription factors (Sakuraba and Yanagisawa, 2018). Nutrients such as nitrogen (N), phosphorus (P), and potassium (K) are linked to numerous plant metabolic pathways and play a pivotal role in conferring tolerance to abiotic stresses by regulating signaling pathways that steer plasticity (Singh et al., 2021; Kumari et al., 2024). Understanding the complex interaction between light and nutrients is vital for predicting plant responses to changing environments and for optimizing crop management practices in a world facing climate change and resource limitations (Poorter et al., 2019; Liu et al., 2022). Fig. 1

Adaptation to light and nutrient availability involves modifications in leaf dynamics and nitrogen assimilation (Hikosaka, 2004). Leaf functional traits such as specific leaf area (SLA), leaf mass area (LMA), and leaf area index (LAI) undergo significant adjustments in response to these signals (Gonçalves et al., 2005; Lu et al., 2020; Parker, 2020). These adaptations are crucial for optimizing light capture, gas exchange, and photosynthetic efficiency. Furthermore, leaf plasticity allows plants to adjust their canopy structure to minimize self-shading and improve photosynthetic resource partitioning between and within leaves in nutrient-limited environments (Hikosaka, 2003; Pearcy et al., 2005; Klodd et al., 2016). This would consequently affect nitrogen assimilation. Nitrate reductase, the first enzyme involved in nitrogen reduction, is light and nitrate-dependent, enabling plants to modulate nitrogen

* Corresponding author.
E-mail address: khairulazreerosli@gmail.com (K.A. Rosli).

https://doi.org/10.1016/j.envexpbot.2024.106044
Received 25 August 2024; Received in revised form 11 November 2024; Accepted 15 November 2024
Available online 22 November 2024

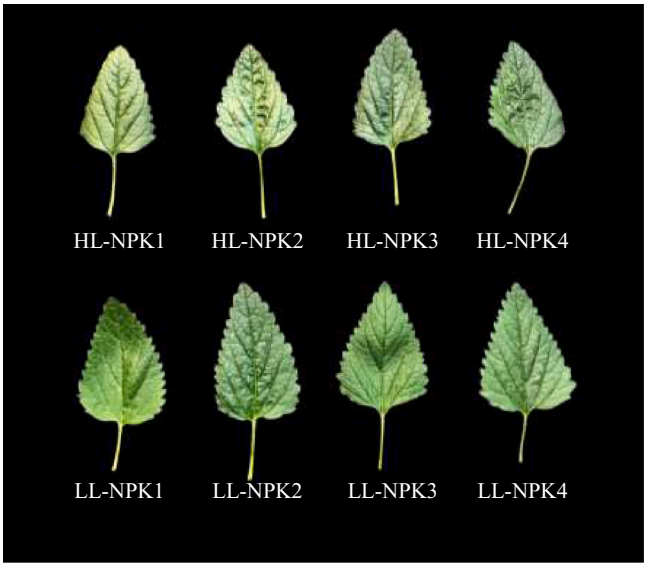

Fig. 1. Leaves of. A. rugosa grown under different light and nutrient levels. Abbreviations: HL, high-light (0 % shade); LL, low-light (50 % shade); NPK1, low-nutrient (40 mg kg^{-1}); NPK2, moderate-nutrient (80 mg kg^{-1}); NPK3, high-nutrient (120 mg kg^{-1}); NPK4, very high-nutrient (160 mg kg^{-1}). The white scale bar represents 3 cm.

uptake in response to environmental fluctuations (Bernacchi et al., 2007; Xu et al., 2012). Changes in nitrogen metabolism coincide with alterations in the absorption and conversion of nitrate (NO_3^-), nitrite (NO_2^-), and ammonium (NH_4^+) (Lillo, 2004; Krapp, 2015). High-light environments can compensate for nitrogen deficit during growth by improving nitrogen use efficiency (Kiba and Krapp, 2016; Esmaeili et al., 2022).

Leaf photosynthetic capacity and energy metabolism are also linked to the availability of light and nutrients (Wu et al., 2019; Shah et al., 2024). Cellular energetics in plants involve the proton pumps, vacuolar H^+-ATPase (V-ATPase) and H^+-pyrophosphatase (V-PPase) working together to sustain vacuolar acidification and energize secondary transport across the tonoplast (Kriegel et al., 2015). Interestingly, their regulation under light and nutrients is still not elucidated. Hence, the integration of cellular energetics with photosynthetic capacity, by estimating parameters such as chlorophyll content and net photosynthesis rate (A) is an aspect of plant adaptation that requires further study. Higher nutrient status enhances photosynthesis and chlorophyll content, improving plants' ability to adapt to high-light conditions (Grassi et al., 2001; Figueroa et al., 2009). However, there is a threshold of light and light supply over which the plant may decrease photosynthetic capacity (Cisse et al., 2020; Pashkovskiy et al., 2021), influencing photosynthetic nitrogen-use efficiency (PNUE). Qiang et al. (2023) observed that photosynthetic rate and PNUE increase with increasing nitrogen levels. Such traits enable plants to balance between investing leaf resources into light-harvesting complexes and carbon assimilation.

Agastache rugosa (Fisch. & C.A.Mey.) Kuntze is a perennial herb, widely valued for its essential oils and phytochemicals (Haiyan et al., 2016; An et al., 2018). This economically important herb is used in pharmaceutical, cosmetic, and food industries (An et al., 2018; Anand et al., 2018; Hou et al., 2022; Kim, 2020; Lee et al., 2020; Yamani et al., 2014), and is commercially grown in subtropical and temperate zones. Despite significant advances in plant physiology, the specific mechanisms by which light-nutrient interactions affect leaf dynamics in relation to nitrogen assimilation and cellular energetics remain inadequately addressed. Previous studies on this species have primarily focused on the main effects of light or nutrient, neglecting their combined influence on major physiological processes (Hyun Choong et al., 2000; Kim et al., 2018; Gardner, 2019; Liu et al., 2022). To address this gap, we hypothesized that *A. rugosa* would modulate its leaf dynamics, nitrogen assimilation, and cellular energetics in response to different light and nutrient combinations. Our objective was to elucidate the responses of *A. rugosa* to the combined effects of light and nutrient, focusing on leaf traits and physiological adjustments and their relationships using multivariate approaches.

2. Materials and methods

2.1. Plant materials

A. rugosa seeds were bought from a local supplier (WHT Wellgrow Seeds, Malaysia). The seeds were surface-sterilized for 1 min with 70 % ethanol, followed by 5 % sodium hypochlorite solution for 10 min, then rinsed thrice with distilled water. The seeds were sown in 200-cell trays containing a 1:1 mixture of blonde peat (Pindstrup Mosebrug A/S, Denmark) and perlite. The seed cell trays were placed on capillary mats under white fluorescent light/dark (16/8 h) photoperiod (Park et al., 2020), in a room maintained at 20–25°C and 50–70 % relative humidity. The substrate was kept moist but not drenched. Seeds were allowed to germinate and grow under these conditions.

2.2. Experimental setup

This experiment was conducted under two north-south oriented polytunnels (10 m long x 6 m wide x 2 m high) with both end-walls and side-walls (1.5 m high) at Farm 10, Faculty of Agriculture, Universiti Putra Malaysia from September to December 2020. The polytunnels were enclosed with a single layer of transparent polyethylene film (280 microns thick). The end-walls were open, and side-walls were rolled down during the experimental period. To simulate low-light conditions, one tunnel roof was covered externally with a single layer of 50 % black net (Supplementary Fig. S1). Photosynthetic photon flux density (PPFD), air temperature (T_{Air}), and relative humidity (RH) data were recorded using a portable light meter (LI-189, LI-COR, Lincoln, NE, USA) and dataloggers (Supplementary Fig. S2). Six-week-old seedlings of uniform size with four to five true leaves were transplanted to black polythene pots (15 cm diameter x 25 cm high) containing ~3.5 kg pot^{-1} (~24 cm depth) of 3:2:1 potting mix (Universiti Agriculture Park, Serdang, Malaysia). Details on the chemical properties of the potting mix are listed in Table S1. The pots were carefully arranged in the polytunnels spaced 30 cm apart.

Four nutrient levels based on NPK (16:16:16); low (NPK1, 40 mg kg^{-1}, 1.26 g), moderate (NPK2, 80 mg kg^{-1}, 2.52 g), high (NPK3, 120 mg kg^{-1}, 3.78 g) and very high (NPK4, 160 mg kg^{-1}, 5.04 g) were nested under two light levels; high-light (HL, 0 % shade) and low-light (LL, 50 % shade). Granular compound fertilizer (YaraMila, Norway) was used as source of nutrients, hand-applied in individual holes (5 cm deep). Plants were watered after each nutrient application using drip irrigation. Nutrient levels were arranged in a randomized complete block design with four replicates in two sets (4 replicates x 8 treatment combinations x 2 sets = 64 pots) running concurrently. The first set was used for leaf trait measurements, while the second was for physio-biochemical and molecular assays. Light treatments were started at transplanting or 0 days after transplanting, while nutrients were split-applied 6, 13, 27, 41, 55, and 69 days after transplanting. The plants were irrigated to field capacity. Irrigation frequency was adjusted depending on the weather and the stage of plant growth. On sunny days, the drip irrigation was turned on twice a day at 08:00 and 17:00, each for 15 min. The average flow rate was 20 mL/min.

2.3. Leaf trait measurements

Leaves were harvested 84 days after transplanting in the morning and transported to the laboratory. Total leaf area (LA) of detached leaves was measured using a leaf area meter (LI-3100C, LI-COR, Lincoln, NE,

USA). Samples were oven-dried at 105 °C for 30 min, followed by 80 °C for two days (Memmert UNB-500, Germany). Leaf (DWL) and total (DWT) dry weights were recorded. Specific leaf area (SLA), leaf mass area (LMA), leaf mass fraction (LMF) (Hunt, 2012), and leaf area index (Röver and Koch, 1995) were calculated as:

$$SLA\ (cm^2\ g^{-1}) = LA / DWT$$

$$LMA\ (g\ m^{-2}) = DWT / LA$$

$$LMF\ (g^{\ day-1}) = DWL / DWT$$

$$LAI = A / DWL \times Y$$

where A is leaf area (m^2), and Y is total leaf dry weight per surface area of potting mix (g m^{-2}).

2.4. Photosynthetic capacity and resource use efficiency

Fully expanded leaves (the third or the fourth from the apex) were used for the relative chlorophyll content and photosynthesis rate measurements. Relative chlorophyll content was determined using a chlorophyll meter (SPAD-502, Minolta Co. Ltd., Japan), expressed as SPAD values (Wicharuck et al., 2024). Net photosynthesis rates (A) were determined on the exact spots of the SPAD readings using a photosynthesis device (LI-6800, LI-COR Incorporated, Lincoln, NE, USA) equipped with a 6 cm^2 leaf chamber with controlled light and gas flow (6800–01 A). The instrument was calibrated and set to measure at an ambient CO_2 concentration of 400 µmol/mol, 50–60 % relative humidity, 1500 µmol m^{-2} s^{-1} PPFD, and airflow rate of 500 µmol air s^{-1}. Data were recorded at steady-state conditions in between measurements. The leaves were collected, oven-dried at 70°C for 24 h, and powdered in an electric stainless-steel grinder (Nima NM-8300, Japan) to pass a 300-mesh sieve (Motsara and Roy, 2008). Ground samples (0.25 g) were liquefied through wet acid digestion with 5 mL of sulfuric acid and hydrogen peroxide. The resulting digest solutions were tested for total nitrogen calorimetrically (Koistinen et al., 2019). Photosynthetic nitrogen use efficiency (PNUE) (Ye et al., 2019) were calculated as:

$$PNUE\ (^{\mu mol}\ CO_2\ mol^{-1}\ N\ s^{-1}) = A / N$$

where N is the total nitrogen content per leaf area (g N m^{-2}).

2.5. Nitrate reductase activity

In-vivo nitrate reductase activity (NR, EC 1.7.99.4) was determined following a modified method (Adavi et al., 2019). In the morning, twenty leaf disks were collected from similar leaves previously measured for SPAD and A, using a single-hole punch, and placed into falcon tubes. Samples were transported to the laboratory in a cooler with ice packs. Next, 3 mL of ice-cold incubation medium (0.1 M phosphate buffer pH 7.5, 0.4 M KNO_3, plus n-propanol) was pipetted into each tube, and the samples were sonicated for 15 min using an ultrasonic bath (37 kHz, Fisherbrand™ FB15055, Fisher Scientific, UK). Samples were kept cool during sonication by placing ice packs in the bath. Samples were vacuum infiltrated for 5 min at −25 inHg until all leaf disks sank to the bottom when the vacuum was released. Samples were incubated in a water bath (WiseBath®, Daihan Scientific, Co., Ltd, Seoul, Korea) at 35°C for 30 min in the dark, boiled for 5 min, and left to cool. Next, 1 mL of samples was added into fresh falcon tubes, plus 1 mL each of 1 % sulfanilamide and 0.02 % N-(1-Naphthyl) ethylenediamine dihydrochloride (NEDD). The mixtures were incubated for 20 min at room temperature (20–25°C) until a pink color developed and adjusted with ultrapure water to get 10 mL final volume. Absorbance was read at 540 nm using a spectrometer (Multiskan GO, Thermo Scientific, Waltham, USA) and compared to a sodium nitrite standard. Nitrate reductase activity was expressed as micromoles of nitrite formed per area per hour (µmol NO_2 cm^{-2} h^{-1}).

2.6. Fresh sample preparation

For nitrogen compounds and proton pump assays, leaf samples (the third or fourth from the apex) were flash-frozen at harvest, powdered with liquid nitrogen using precooled porcelain mortars and pestles, and stored at −80°C until use (MDF-U55V-PE, Panasonic, Japan).

2.7. Nitrate

Nitrate (NO_3^-) content was determined using the spectrometric method with some modifications (Hachiya and Okamoto, 2017). Frozen samples were weighed into microtubes at 0.1 g each and pipetted with 1 mL of ultrapure water. Samples were boiled in a water bath for 20 min, left to cool, and centrifuged (ScanSpeed 1730 R, LaboGene™, Denmark) at 24°C for 10 min at 8,000x*g*. Next, 10 µL of supernatants and standards were pipetted with 40 µL of 0.05 % salicylic acid in sulfuric acid into fresh microtubes. Sulfuric acid was pipetted at 40 µL into another microtube to serve as blank. Mixtures were vortexed and incubated at room temperature for 20 min. Then, 1 mL of 8 % sodium hydroxide solution was pipetted into the tubes. In a 96-well microplate, 200 µL of samples, standards, and blank were pipetted into the wells. Absorbance was read at 410 nm and compared to a potassium nitrate standard. Nitrate content was expressed as micromoles per gram tissue fresh weight (µmol g^{-1} FW).

2.8. Nitrite

Nitrite (NO_2^-) content was determined using the spectrometric method with some modifications (Hachiya and Okamoto, 2017). Frozen samples were weighed into microtubes at 0.1 g each and homogenized with 1 mL of ice-cold extraction buffer (1 mM EDTA, 7 mM L-cysteine in 50 mM HEPES-KOH pH 7.6) using a mini homogenizer (LabGEN 7, Cole-Palmer, USA). Homogenates were centrifuged at 4°C for 10 min at 8,000x*g*. Samples were kept cold using a microtube cooler (R1000 Durastar Polymer CoolCube, Benchmark Scientific, USA). Next, 200 µL of supernatants and standards were pipetted with 100 µL of 1 % sulfanilamide in hydrochloric acid into fresh tubes. The mixtures were centrifuged at 4°C for 10 min at 8,000x*g*. In a 96-well microplate, 200 µL of samples, standards, and blank were pipetted into the wells. Next, 100 µL of 2 % NEDD solution was added into the wells for color development. Absorbance was read at 540 nm and compared to a sodium nitrite standard. Nitrite content was expressed as nanomoles per gram tissue fresh weight (nmol g^{-1} FW).

2.9. Ammonium

Ammonium (NH_4^+) content was determined using the spectrometric method (Vega-Mas et al., 2015) with some modifications. Similar supernatants from nitrate determination were used for this assay. In a 96-well microplate, 50 µL of samples, standards, and blank were pipetted into the wells. Next, 100 µL of reaction mixture (0.33 M sodium phenolate in 2 M sodium hydroxide and 0.5 % sodium nitroprusside) was pipetted into each well and incubated at room temperature for 30 min for color development. Absorbance was measured at 635 nm and was compared to an ammonium nitrate standard. Ammonium content was expressed as micromoles per gram tissue fresh weight (µmol g^{-1} FW).

2.10. Nitrate/nitrite and nitrate/ammonium ratios

Nitrate/nitrite (NO_3^-/NO_2^-) and nitrate/ammonium (NO_3^-/NH_4^+) ratios were calculated by dividing NO_3^- with the resulting NO_2^- and NH_4^+ concentrations.

2.11. Proton pump activity

The hydrolytic activities of two electrogenic proton pumps, vacuolar H^+-ATPase (V-ATPase, EC 3.6.3.14) and H^+-pyrophosphatase (V-PPase, EC 3.6.1.1) were determined by measuring inorganic phosphate release (Bernado et al., 2022). Microsomal fractions containing tonoplast were isolated using differential centrifugation. Frozen samples were weighed into falcon tubes at 0.5 g each and homogenized with 10 mL of ice-cold homogenization buffer (350 mM sucrose, 3 mM disodium EDTA, 10 % glycerol, 0.15 % BSA, 1.5 % PVP-40, 4 mM DTT and 5 μg/mL chymostatin (dissolved in DMSO at 10 mg/mL) in 70 mM Tris-HCL pH 8.0). Homogenates were filtered through two layers of nonwoven gauze with gentle hand pressure and centrifuged at 4°C for 15 min at 15,000x*g*. The supernatants were collected and filtered again through a layer of nonwoven gauze into 13.2-mL polyallomer tubes (#331372, Beckman Coulter, Palo Alto, USA). The samples were centrifuged in an Optima L-100 XP ultracentrifuge fitted with a SW41Ti swinging bucket rotor at 100,000x*g* (~24,200 rpm) for 1 h with maximum acceleration and deceleration (Beckman Coulter, CA, k-factor: 356) at 4 °C. The pellets were resuspended in 1 mL of suspension buffer (350 mM sucrose, 2 mM DTT, 5 μg/mL chymostatin in 10 mM Tris-MES pH 7.0). The resulting microsomal suspensions were stored in a freezer at −80°C until use.

For the V-ATPase assay, 50 μL of microsomal suspensions were pipetted into 2-mL microtubes. Next, 200 μL of ice-cold reaction medium (4 mM $MgSO_4$, 50 mM KCL, 1 mM NaN_3, 0.1 mM Na_2MoO_4, 0.1 % Brij 35, 500 μM Na_3VO, and 2 mM ATP-Na_2 in 25 mM Tris-MES pH 7.0) were pipetted into the samples and control tubes, incubated at 30°C for 40 min in an oven. Pi release from ATP hydrolysis was measured with and without adding 20 μL of 100 nM Concanamycin A (dissolved in DMSO). The reaction was stopped by pipetting 160 μL of 40 mM citric acid. The assay mixtures were reacted with 550 μL of 0.905 % Na_2MoO_4 in 1.45 N HCL and 40 μL of 0.05 % ANSA solution. For the V-PPase assay, 100 μL of microsomal suspensions were pipetted into 2-mL microtubes. Next, 200 μL of ice-cold reaction medium (2 mM $MgSO_4$, 0.1 mM Na_2MoO_4, 0.1 % Brij 58, 0.2 mM potassium pyrophosphate in 25 mM Tris-MES pH 7.5) were pipetted into samples and control tubes, and incubated at 30°C for 40 min in an oven. For controls, 20 μL of 50 mM potassium chloride was pipetted before adding the suspensions. The reaction was terminated by adding 160 μL of 40 mM citric acid. The mixtures were further reacted with 550 μL of 0.905 % sodium molybdate in 1.45 N HCL and 40 μL of 0.05 % ANSA solution. In a 96-well flat bottom microplate, 200 μL of samples, controls, and blank were pipetted into the wells. Absorbance was read at 700 nm. Both V-ATPase and V-PPase activities were expressed as percentages using the following equation:

$$\% \text{ V-ATPase} = [(A_{sample} - A_{blank}) - (A_{control} - A_{blank})] / (A_{control} - A_{blank}) \text{ x } 100$$

Where ^{Asample}= absorbance of sample

A_{blank}= absorbance of blank

$A_{control}$= absorbance of control

2.12. Statistical analysis

Data were analyzed using SAS® version 9.4 by the general linear model (PROC GLM). Wherever necessary, data was transformed before analysis through Box-Cox transformations to ensure the normality of residuals was satisfied. A combined analysis of variance was performed for the four nutrient levels nested under light levels (Bowley, 1999; Moore and Dixon, 2015). The means of significant main effects and interactions were separated with the least significant difference (LSD) posthoc test (Vargas et al., 2015). Pearson's correlation test, principal component analysis (PCA), and hierarchical cluster analysis (HCA) were used to explore the relationship among variables and group them based on their similarities. Graphs, heatmap, dendrogram, and biplot after PCA were made using OriginPro® 2024b.

3. Results

3.1. Leaf dynamics

Light and nutrient interactions significantly influenced leaf traits ($P < 0.05$) of *A. rugosa*. Specific leaf area (SLA, Fig. 2A) exhibited consistently higher values under low-light conditions across all nutrient levels, with LL-NPK1 exhibiting the highest value (302.70 ± 15.34 $cm^2\ g^{-1}$), representing a 91 % increase compared its high-light counterpart (158.92 ± 11.89 $cm^2\ g^{-1}$). SLA increased by 42 % under LL-NPK2 (261.50 ± 11.21 $cm^2\ g^{-1}$) compared to HL-NPK2 (184.82 ± 9.58 $cm^2\ g^{-1}$). Leaf mass area (LMA, Fig. 2B) showed an inverse relationship, with high-light conditions yielding greater values, particularly in HL-NPK1 (63.19 ± 4.68 $g\ m^{-2}$), which was 97 % higher than LL-NPK1 (32.10 ± 1.71 $g\ m^{-2}$). This difference diminished with increasing nutrient levels, displaying only a 42 % difference at NPK4. LMA was higher by 44 % under HL-NPK3 (56.68 ± 5.03 $g\ m^{-2}$) than its high-light counterpart (39.39 ± 1.22 $g\ m^{-2}$). Leaf mass fraction (LMF, Fig. 2C) peaked at LL-NPK1 (0.53 ± 0.08 $g\ g^{-1}$), exhibiting a 33 % increase over HL-NPK1 (0.42 ± 0.02 $g\ g^{-1}$), with subsequent nutrient levels showing diminishing differences between light treatments, finally converging at NPK4 (HL: 0.43 ± 0.01; LL: 0.41 ± 0.01 $g\ g^{-1}$; 5 % difference). Leaf area index (LAI, Fig. 2D) demonstrated a progressive increase with nutrient levels under both light conditions with low-light environments showing a 48 % higher LAI than high-light conditions at NPK1. Notably, this pattern reversed at NPK4, where high-light conditions produced a markedly higher LAI (6.68 ± 0.21), representing a 9 % increase compared to low-light levels (6.17 ± 0.14). The response to nutrient supply was most distinct between NPK1 and NPK2, with NPK2 exhibiting a 16 % increase in SLA and 14 % decrease in LMA than NPK1 in high-light environments, while subsequent nutrient increments (NPK3 and NPK4) resulted in changes of less than 10 %.

3.2. Nitrogen reduction/assimilation

Interaction effects ($P < 0.05$) were observed between different light and nutrient levels on nitrogen reduction/assimilation parameters in *A. rugosa*. Nitrate reductase (NR, Fig. 3A) activity exhibited a distinct pattern, with HL-NPK4 exhibiting the highest activity (0.34 ± 0.02 μmol $NO_2\ cm^{-2}\ h^{-1}$), demonstrating a 62 % increase compared to LL-NPK4 (0.21 ± 0.01 μmol $NO_2\ cm^{-2}\ h^{-1}$). Nitrate (NO_3^-, Fig. 3B) content showed an inverse relationship with increasing nutrient levels, where HL-NPK1 maintained the highest concentration (13.89 μmol g^{-1} FW), approximately 15 % higher than under LL-NPK1 (12.13 ± 0.25 μmol g^{-1} FW), followed by a gradual decline of up to 48 % across treatments. Nitrite (NO_2^-, Fig. 3C) accumulation was significantly elevated in HL-NPK2 (35.87 ± 1.49 nmol g^{-1} FW), LL-NPK3 (34.88 ± 2.69 nmol g^{-1} FW), and LL-NPK4 (37.83 ± 2.07 nmol g^{-1} FW) leaves, showing an 81 % increase compared to the lowest values observed in NPK1 treatment. Ammonium (NH_4^+, Fig. 3D) content peaked under LL-NPK1 (0.99 ± 0.04 μmol g^{-1} FW), nearly 7 % higher than HL-NPK1, and exhibited a decreasing trend of up to 65 % with nutrient levels in both light conditions. NO_3^-/NO_2^- ratio (Fig. 3E) was highest under HL-NPK1 (1.0) and showed a consistent decrease of up to 75 % with declining nutrients in low-light conditions. Notably, NO_3^-/NH_4^+ ratio (Fig. 3F) reached its maximum under LL-NPK3 (41.3), representing a 205 % increase compared to HL-NPK1 and LL-NPK1, which had the lowest ratios (~14), and displayed similar patterns across several light and nutrient treatment combinations.

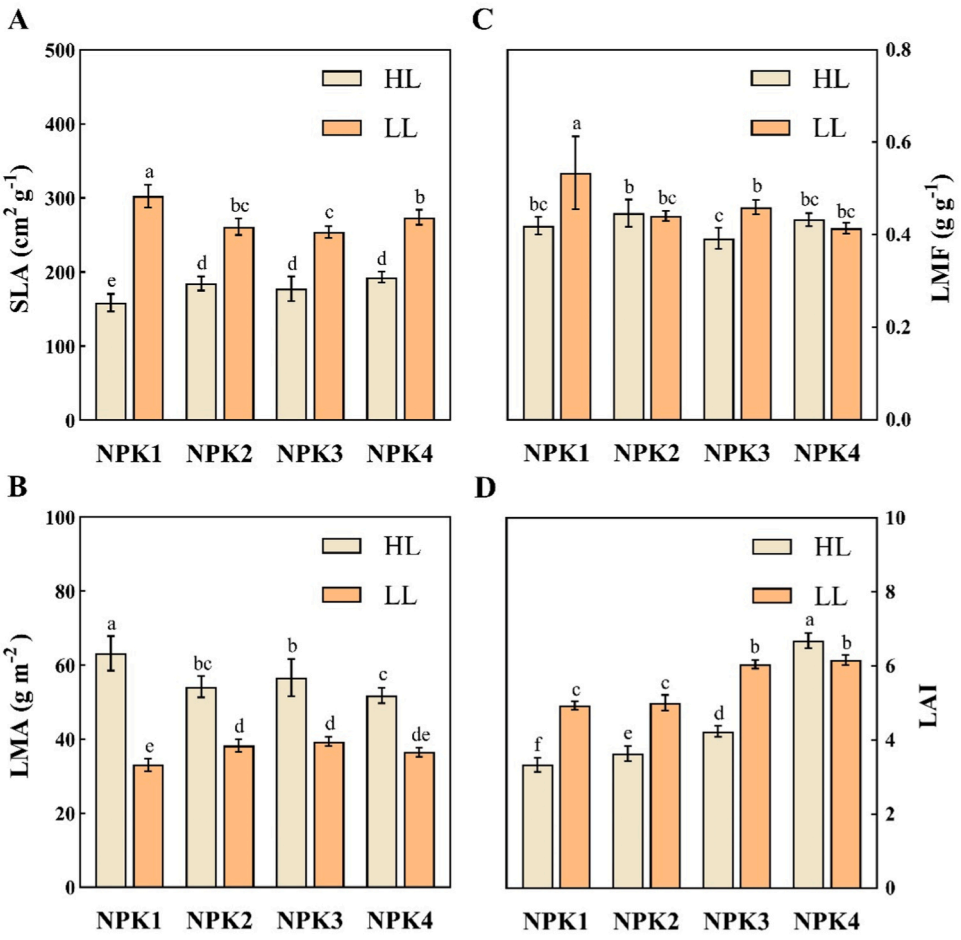

Fig. 2. Leaf dynamics of A. rugosa under different light and nutrient levels. Abbreviations: HL, high-light (0 % shade); LL, low-light (50 % shade); NPK1, low-nutrient (40 mg kg^{-1}); NPK2, moderate-nutrient (80 mg kg^{-1}); NPK3, high-nutrient (120 mg kg^{-1}); NPK4, very high-nutrient (160 mg kg^{-1}); SLA, specific leaf area; LMA, leaf mass area; LMF, leaf mass fraction; LAI, leaf area index. The vertical bars are mean ± SD (n = 4). Different letter(s) above bars indicate significant differences according to LSD. LSD = Least significant difference; SD = Standard deviation.

3.3. Photosynthetic capacity and resource use efficiency

Single and interaction effects of light and nutrient ($P < 0.05$) were observed on the photosynthetic capacity and resource use efficiency in *A. rugosa*. Relative chlorophyll content (SPAD, Fig. 4A) increased by 9 % under high-light treatment (53.11 ± 3.94) compared to low-light levels (48.67 ± 3.60), while nutrient levels did not affect them. Significant interaction effects were observed for net photosynthesis rate (A, Fig. 4B) and photosynthetic nitrogen use efficiency (PNUE, Fig. 4C). Under NPK1 and NPK2, both light treatments showed similar A values (~12 μmol CO_2 m^{-2} s^{-1}). However, at higher nutrient levels, A increased differentially with HL-NPK3 leaves exhibiting the highest A (17.62 ± 0.89 μmol CO_2 m^{-2} s^{-1}), representing a 50 % increase from NPK1 levels, while LL-NPK4 demonstrated a 42 % increase (16.41 ± 0.90 μmol CO_2 m^{-2} s^{-1}) compared to LL-NPK1. Notably, PNUE displayed a contrasting pattern, with low-light leaves consistently outperforming high-light across all nutrient treatments. This difference was most pronounced under NPK2, where low-light conditions resulted in a 451 % higher PNUE (64.45 ± 6.92 μmol CO_2 mol^{-1} N s^{-1}) than high-light levels (11.69 ± 0.74 μmol CO_2 mol^{-1} N s^{-1}). The PNUE values gradually decreased with increasing nutrient levels in low-light conditions, declining by 43 % from NPK2 to NPK4 (64.4–36.8 μmol CO_2 mol^{-1} N s^{-1}), while remaining relatively stable under high-light conditions (11.69–15.01 μmol CO_2 mol^{-1} N s^{-1}), showing only minor fluctuations of ±16 %.

3.4. Cellular energetics

Light and nutrients showed interactions ($P < 0.05$) for both vacuolar proton pumps in *A. rugosa*. For vacuolar H^+-ATPase (V-ATPase, Fig. 5A) activity, high-light with moderate nutrient levels (HL-NPK2) yielded the highest activity (15.6 %), representing a 46 % increase over the lowest observed activity under LL-NPK1 (10.8 %). While subsequent nutrient increases under high-light (HL-NPK3 and HL-NPK4) maintained relatively high activities (~14.5 %), they exhibited a 7 % decrease from the peak HL-NPK2 level. Under low-light conditions, V-ATPase activity peaked at moderate to high nutrients (LL-NPK2 and LL-NPK3, ~14.5 %), showing a 35 % increase from LL-NPK1, but declined by 15 % at LL-NPK4. V-PPase activity showed more dramatic fluctuations, with HL-NPK2 and HL-NPK3 recording the highest activities (53.1 % and 52.4 %, respectively), displaying an 86 % increase over the lowest observed activity in LL-NPK4 (28.6 %). Under low-light conditions, V-PPase activity demonstrated a downward trend with increasing nutrient levels, declining by 30 % from LL-NPK1 (41.1 %) to LL-NPK4 (28.6 %). High-light levels maintained 18–33 % higher proton pump activities than their low-light counterparts across most nutrient levels.

3.5. Correlations among measured traits

The heatmap reveals complex relationships between leaf traits, nitrogen metabolism, and cellular energetics in *A. rugosa* under varying light and nutrient levels (Fig. 6). Strong negative correlation exists

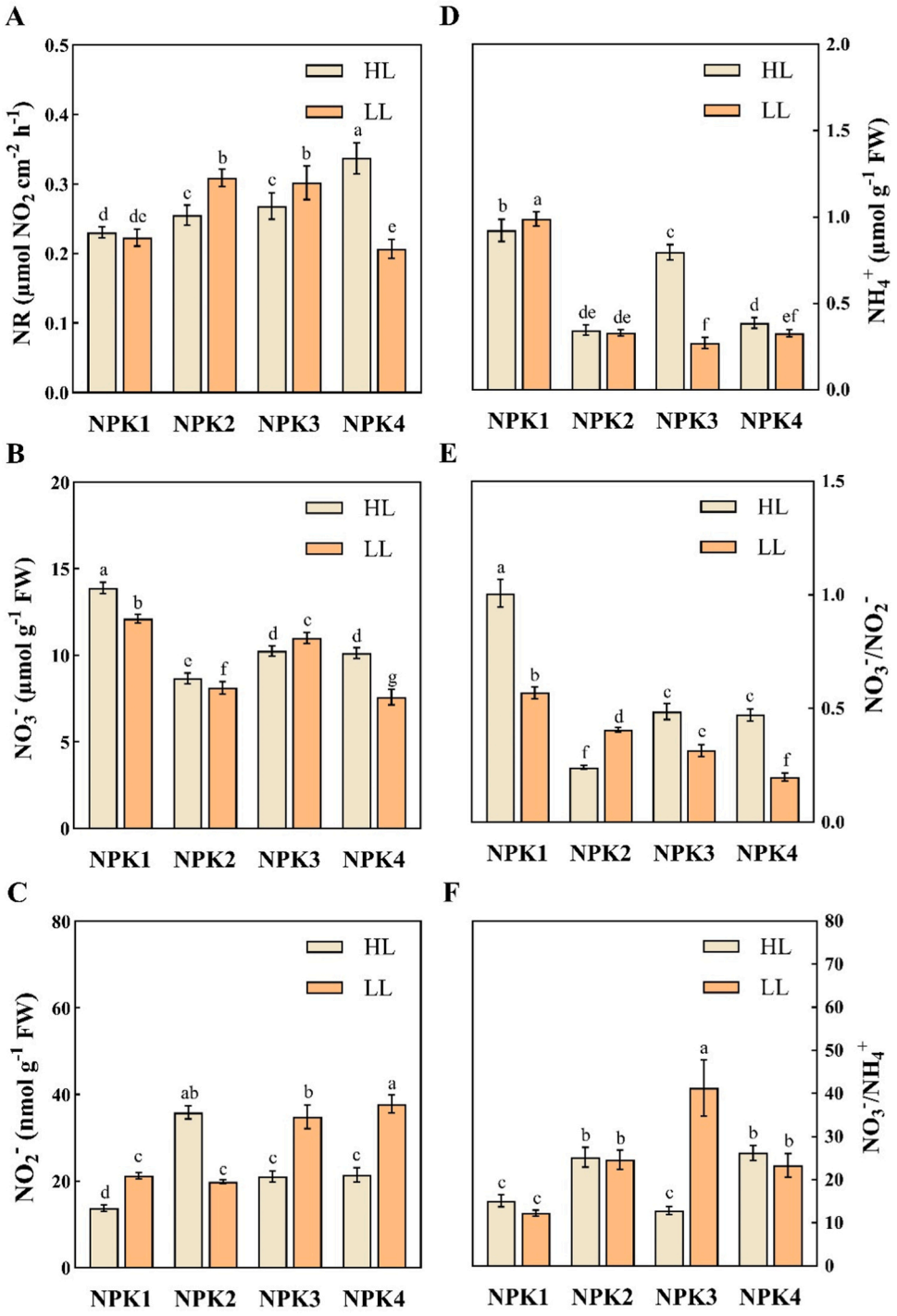

Fig. 3. Nitrogen reduction/assimilation in A. rugosa under different light and nutrient levels. Abbreviations: HL, high-light (0 % shade); LL, low-light (50 % shade); NPK, low-nutrient (40 mg kg^{-1}); NPK2, moderate-nutrient (80 mg kg^{-1}); NPK3, high-nutrient (120 mg kg^{-1}); NPK4, very high-nutrient (160 mg kg^{-1}); NR, nitrate reductase; NO_3^- nitrate; NO_2^-, nitrite; NH_4^+, ammonium; NO_3^-/NO_2^-, nitrate/nitrite ratio; NO_3^-/NH_4^+, nitrate/ammonium ratio. The vertical bars are mean ± SD (n = 4). Different letter(s) above bars indicate significant differences according to LSD. LSD = Least significant difference; SD = Standard deviation.

between SLA and LMA (r = −0.98) as expected, while NO_3^- demonstrates strong positive correlation with NH_4^+ (r = 0.73). NO_3^-/NO_2^- ratio exhibits strong positive correlations with both NO_3^- (r = 0.85) and NH_4^+ (r = 0.75), and NO_3^-/NH_4^+ ratio shows strong negative correlation with NH_4^+ (r = −0.82). Moderate correlations include negative relationships between LMA and both LAI (r = −0.56) and PNUE (r = −0.64), LMF with A (r = −0.52), and NO_2^- with NO_3^- (r = −0.58), while positive moderate correlations exist between LAI and NO_3^-/NH_4^+ ratio (r = 0.51), SPAD readings and V-ATPase (r = 0.56), NR with V-ATPase (r = 0.63) and NO_3^-/NH_4^+ ratio (r = 0.46), and V-ATPase with V-PPase (r = 0.46). Weak but significant correlations include SLA with LMF (r = 0.45) and LAI (r = 0.49), SPAD with LMA (r = 0.38), and NO_3^- and NO_2^- with LMA (r = 0.36 and r = −0.36, respectively). LMF showed weak direct correlations with nitrogen forms (r < 0.30). Fig. 7

3.6. Principal component analysis of measured traits

The PCA biplot reveals distinct clustering patterns of physio-

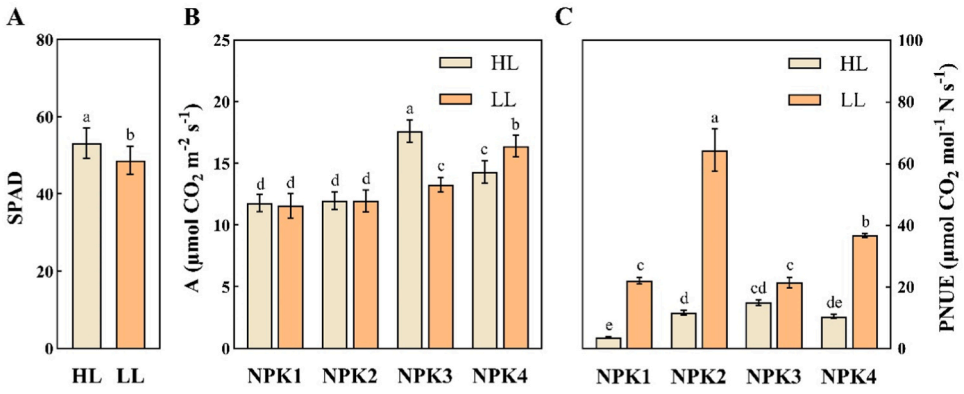

Fig. 4. Single and interaction effects of light and nutrient on photosynthetic capacity and resource use efficiency of A. rugosa. Abbreviations: HL, high-light (0 % shade); LL, low-light (50 % shade); NPK1, low-nutrient (40 mg kg^{-1}); NPK2, moderate-nutrient (80 mg kg^{-1}); NPK3, high-nutrient (120 mg kg^{-1}); NPK4, very high-nutrient (160 mg kg^{-1}); SPAD, relative chlorophyll content A, net photosynthesis rate; PNUE, photosynthetic nitrogen use efficiency. The vertical bars are mean ± SD (n = 4). Different letter(s) above bars indicate significant differences according to LSD. LSD = Least significant difference; SD = Standard deviation.

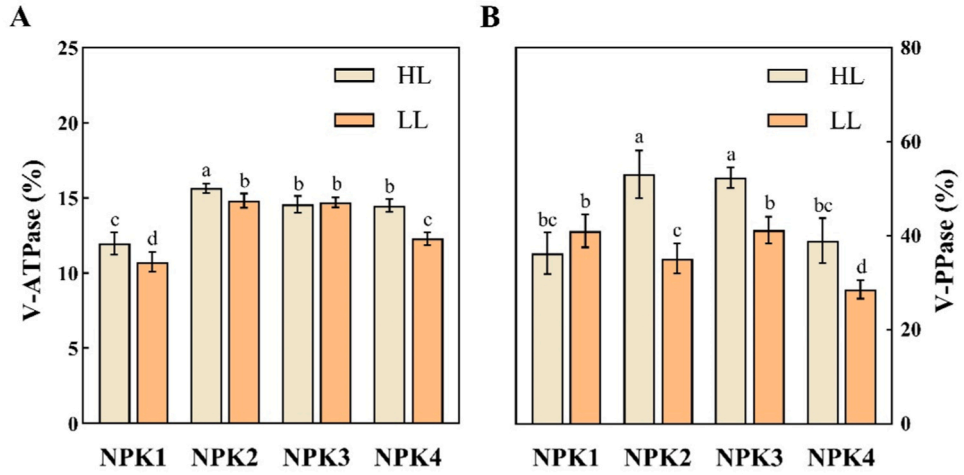

Fig. 5. Proton pump activity in A. rugosa under different light and nutrient levels. Abbreviations: HL, high-light (0 % shade); LL, low-light (50 % shade); NPK1, low-nutrient (40 mg kg^{-1}); NPK2, moderate-nutrient (80 mg kg^{-1}); NPK3, high-nutrient (120 mg kg^{-1}); NPK4, very high-nutrient (160 mg kg^{-1}); V-ATPase, vacuolar H^+-ATPase; V-PPase, vacuolar H^+-pyrophosphatase. The vertical bars are mean ± SD (n = 4). Different letter(s) above bars indicate significant differences according to LSD. LSD = Least significant difference; SD = Standard deviation.

biochemical traits in *A. rugosa* under different light and nutrient levels, with the first two components explaining 58.4 % of total variance (Dim1: 34.3 %, Dim2: 24.1 %). High-light and low-light treatments showed clear separation along both dimensions, with high-light conditions (HL-NPK2, HL-NPK3, and HL-NPK4) clustering in the upper-right quadrant. Nitrogen-related traits (NO_3^-, NH_4^+, and NO_3^-/NO_2^-) grouped tightly on the negative side of Dim1 (-1.5 to −2.0), displaying strong association with HL-NPK1 treatment. Meanwhile, energy and nitrogen metabolism enzymes (V-ATPase, V-PPase, and NR) along with photosynthetic traits (SPAD, A) displayed strong positive correlations with Dim1 (0.5–1.0) and moderate positive correlations with Dim2 (0.5–1.5), aligning more closely with higher nutrient treatments under high light. Leaf morphological traits showed distinct patterns with LMA vectors oriented toward the upper-left quadrant (~ −0.5, 1.2), while its inverse parameter SLA positioned in the lower-right quadrant (~ 1.0, −1.5). PNUE and LAI showed negative correlations with both dimensions, clustering with low-light and high-nutrient treatments (LL-NPK3 and LL-NPK4) in the lower-right quadrant. NO_3^-/NH_4^+ ratio and NO_2^- vectors extended toward positive Dim1 (1.0–1.5), indicating relations to higher nutrient levels, while LMF showed independent orientation with a unique downward vector (~ 0, −1.0).

3.7. Cluster analysis of selected traits

The HCA dendrogram reveals three distinct clusters that match the PCA biplot spatial groupings with dissimilarity distances ranging from 0 to 100 (Fig. 8). The first cluster (purple, lower right quadrant of biplot) contains SLA and PNUE with the highest similarity (80 %), connecting to LAI (70 %), then to NO_2^- and NO_3^-/NH_4^+ (65 %). The second cluster (blue, upper right quadrant of biplot) shows V-PPase and SPAD at highest similarity (70 %) forming a subgroup with NR, then joining V-ATPase (65 %), and finally connecting to LMA (60 %) and A (55 %). The third cluster (green, left side of biplot) exhibits the highest similarity between NO_3^- and NO_3^-/NO_2^- (90 %), then joins with NH_4^+ (85 %), and connects to LMF (70 %). At the broadest level, the blue and green clusters merge (40 %), while the purple cluster connects to these combined groups at the lowest similarity (20 %). Fig. 9

4. Discussion

The interplay between leaf dynamics, nitrogen metabolism, and cellular energetics in *A. rugosa* reveals previously unreported adaptive strategies under different light and nutrient levels. The clustering of leaf mass fraction (LMF), nitrate/nitrite ratio (NO_3^-/NO_2^-), and ammonium (NH_4^+) imply a coordinated response in nitrogen assimilation and

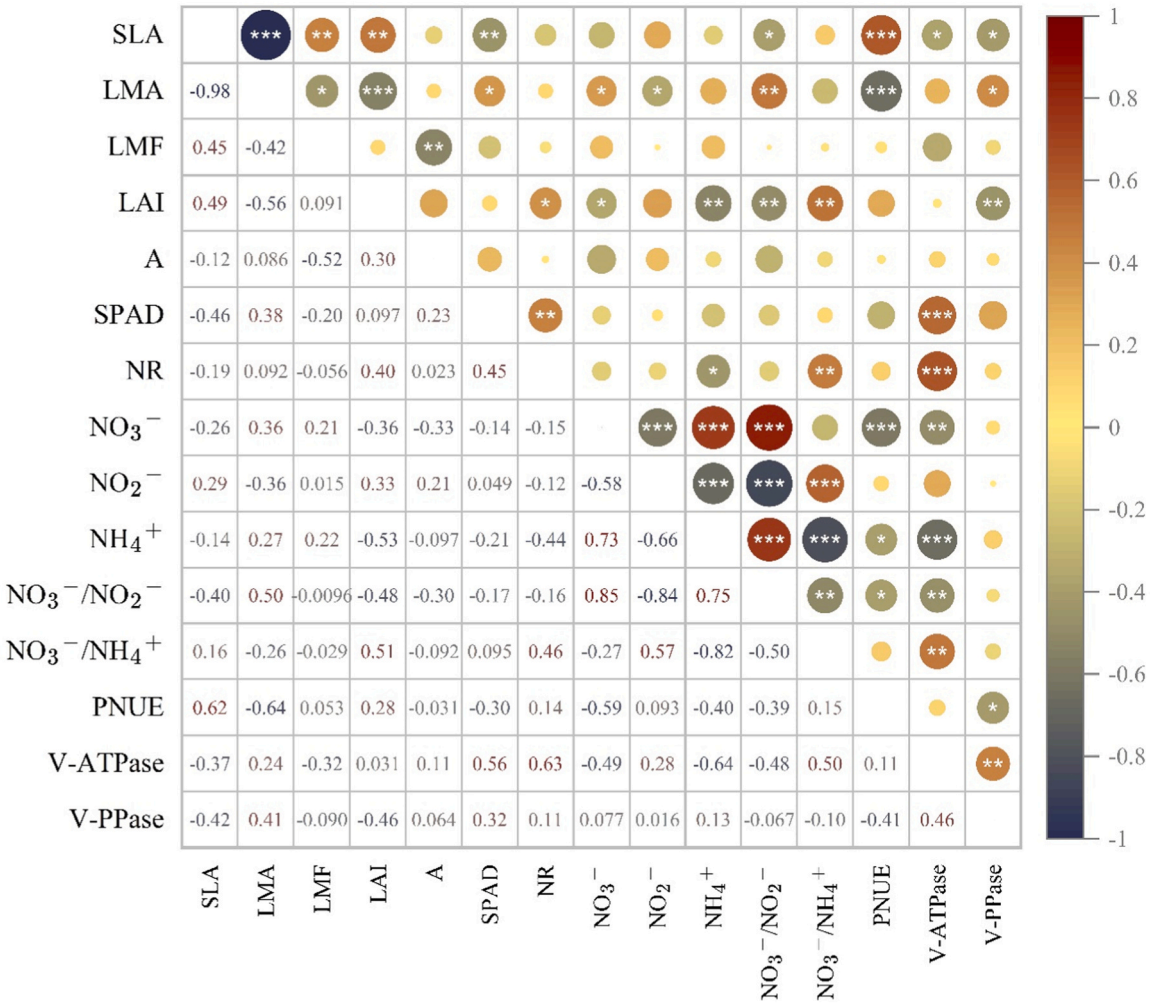

Fig. 6. Heatmap showing correlations between traits related to leaf dynamics, nitrogen assimilation, and cellular energetics in A. rugosa grown under different light and nutrient levels. Abbreviations: SLA, specific leaf area; LMA, leaf mass area; LMF, leaf mass fraction; LAI, leaf area index; A, net photosynthesis rate; SPAD, relative chlorophyll content; NR, nitrate reductase; NO_3^-, nitrate; NO_2^-, nitrite; NH_4^+, ammonium; NO_3^-/NO_2^-, nitrate/nitrite ratio; NO_3^-/NH_4^+, nitrate/ammonium ratio; PNUE, photosynthetic nitrogen use efficiency; V-ATPase, vacuolar H^+-ATPase; V-PPase, vacuolar H^+-pyrophosphatase (***$P < 0.001$; **$P < 0.01$; *$P < 0.05$).

allocation within leaves. The strong positive correlation between NO_3^- and NH_4^+ at high-light and low-nutrient levels, coupled with negative correlation between NO_2^- and NO_3^- reveals an active metabolic state where *A. rugosa* adjusts nitrogen metabolism by maintaining balanced pools of different nitrogen forms. This can be achieved via enhanced nitrogen uptake, altered assimilation pathways, or improved nitrogen storage (Tegeder and Masclaux-Daubresse 2018; Li et al., 2021; Akhtar et al., 2024). The inverse relationship between NO_2^- and NO_3^- also indicates enhanced nitrate reduction capacity, possibly as a mechanism to prevent NO_2^- accumulation which can be detrimental to plant cells (Ezzine and Ghorbel, 2006), suggesting a potential adaptation to nutrient stress. Such complex relationships partly align with the resource optimization theory, which proposes that plants adjust their nitrogen pools and allocation in response to environmental cues (Anten and During, 2011; Quebbeman and Ramirez, 2016). Our findings extend beyond this framework by demonstrating that the adaptive responses of *A. rugosa* are not driven by the main effects of light or nutrients, but by their complex interactions. Multivariate analysis showed that these nitrogen-related traits are closely associated with high-light, low--nutrient levels (HL-NPK1), suggesting that the plant employs unique nitrogen assimilation strategies under these suboptimal conditions. This challenges the traditional view that plants respond primarily to single environmental factors (Poorter et al., 2019). While HCA analysis groups LMF with nitrogen-related traits, correlation analysis reveals a more nuanced picture, with LMF exhibiting weak direct correlations with nitrogen forms ($r < 0.30$) and a moderate negative correlation with net photosynthesis rate. The PCA biplot shows LMF having a unique downward vector orientation, distinct from both nitrogen metabolism and structural trait clusters, suggesting its regulation is partially decoupled from these processes. This independence in LMF response implies that biomass allocation to leaves may follow distinct regulatory pathways less dependent on nitrogen availability or light conditions than previously thought. Such decoupling could allow *A. rugosa* to sustain flexible biomass allocation strategies even when other physiological processes are constrained by resource limitations. Overall, this coordination may signify an adaptive strategy to maintain nitrogen homeostasis in resource-limited environments, although its direct relationship with biomass allocation is less straightforward than previously suggested.

The differential regulation of proton pumps (V-ATPase and V-PPase) at varying combinations of light and nutrient levels provides novel insights into the cellular energetics of *A. rugosa*. The peak activities of both pumps under high-light and moderate to high-nutrient conditions (HL-NPK2 and HL-NPK3) show a coordinated upregulation of energy metabolism to support increased metabolic demands. This observation builds upon previous reports concerning the crucial role of these pumps in cellular homeostasis and nutrient transport (Krebs et al., 2010; Kriegel et al., 2015; Wang et al., 2021). Our findings, however, go further by

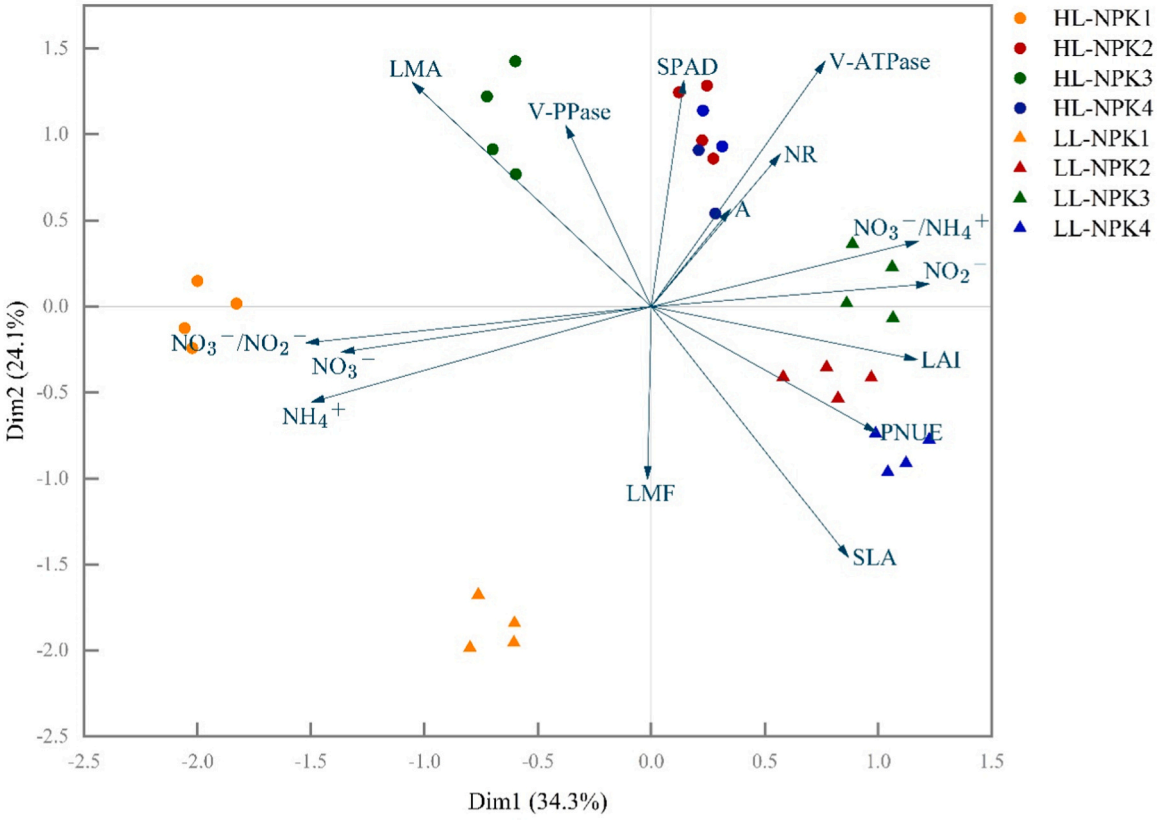

Fig. 7. Principal component analysis (PCA) biplot displaying the relationship among traits related to leaf dynamics, nitrogen assimilation, and cellular energetics in A. rugosa under different light and nutrient levels. Abbreviations: HL, high-light (0 % shade); LL, low-light (50 % shade); NPK, low-nutrient (40 mg kg^{-1}); NPK2, moderate-nutrient (80 mg kg^{-1}); NPK3, high-nutrient (120 mg kg^{-1}); NPK4, very high-nutrient (160 mg kg^{-1}); SLA, specific leaf area; LMA, leaf mass area; LMF, leaf mass fraction; LAI, leaf area index; A, net photosynthesis rate; SPAD, relative chlorophyll content; NR, nitrate reductase; NO_3, nitrate; NO_2, nitrite; NH_4^+, ammonium; NO_3^-/NO_2^-, nitrate/nitrite ratio; NO_3^-/NH_4^+, nitrate/ammonium ratio; PNUE, photosynthetic nitrogen use efficiency; V-ATPase, vacuolar H^+-ATPase; V-PPase, vacuolar H^+-pyrophosphatase.

directly linking the activity of these proton pumps to specific combinations of environmental factors, suggesting a more dynamic and responsive system than previously recognized. Abiotic stresses such as salinity, drought, temperature extremes, acid stress, anoxia, and excess heavy metals in the soil have been shown to depend on maintaining or adjusting the activity of V-ATPase (Dietz et al., 2001). Our findings provide new insights into the relationship between proton pump activity and abiotic stress responses, suggesting that V-ATPase regulation may be a key mechanism involved in tolerance to light and nutrient stress. The HCA analysis further revealed that V-ATPase and V-PPase form distinct subclusters within the broader metabolic response network, with V-ATPase activity showing stronger associations with nitrogen metabolism markers, while V-PPase clusters more closely with structural traits. The clustering of V-PPase and leaf mass area (LMA) suggests that V-PPase regulation is connected to leaf structural adaptations. Higher LMA, typical in high-light environments, often correlates with increased leaf thickness, density, and metabolic activity (Poorter et al., 2009; Kitajima et al., 2016). This response indicates the role of V-PPase in supporting the energetic demands of structurally robust leaves, potentially by maintaining vacuolar pH and turgor pressure (Maeshima, 2001; Segami et al., 2018). The moderate positive correlation between V-ATPase and V-PPase points to a coordinated but not completely redundant function, suggesting distinct roles in cellular energy metabolism in plants. This finding reveals a previously unrecognized specialization in proton pump roles under changing environmental conditions. The temporal dynamics of proton pump activation shown by our PCA loading patterns imply that V-ATPase responds more rapidly to environmental changes compared to V-PPase, potentially acting as an early adaptive response mechanism. The concerted actions of V-ATPase and V-PPase allow *A. rugosa* to adjust its cellular energetics in response to resource availability. This adaptive response may contribute to the species' ability to thrive across diverse habitats.

A key finding of our study is the tight association between specific leaf area (SLA), photosynthetic nitrogen use efficiency (PNUE), leaf area index (LAI), nitrite (NO_2^-), and nitrate/ammonium ratio (NO_3^-/NH_4^+), revealed through novel applications of PCA/HCA analysis. This clustering suggests a complex response involving leaf plasticity, nitrogen use efficiency, and nitrogen metabolism at different light and nutrient levels. The close relationship between SLA and PNUE aligns with previous research showing that leaves with higher SLA tend to have greater nitrogen allocation to photosynthetic machinery, thus increasing PNUE (Schieving and Poorter, 1999; Feng et al., 2008). However, our multivariate analysis distinctively shows that these traits are more closely associated with low-light and high-nutrient conditions (LL-NPK3 and LL-NPK4), suggesting that *A. rugosa* optimizes leaf structure and nitrogen use efficiency in light-limited but nutrient-rich environments.

The inclusion of LAI in this cluster and its position in the PCA biplot further establishes that these leaf-level adaptations scale up to impact canopy-level traits. The association of LAI with NO_2^- and NO_3^-/NH_4^+ ratio suggests a potential mechanism where the balance of different nitrogen forms regulates canopy development. This challenges conventional understanding that often focuses on total nitrogen availability rather than specific nitrogen forms (Xu et al., 2012; Krapp, 2015). Hence, this finding provides new insights into how plants coordinate canopy architecture with nitrogen metabolism at a whole-plant level. The eigenvalue decomposition from our PCA reveals that the first two principal

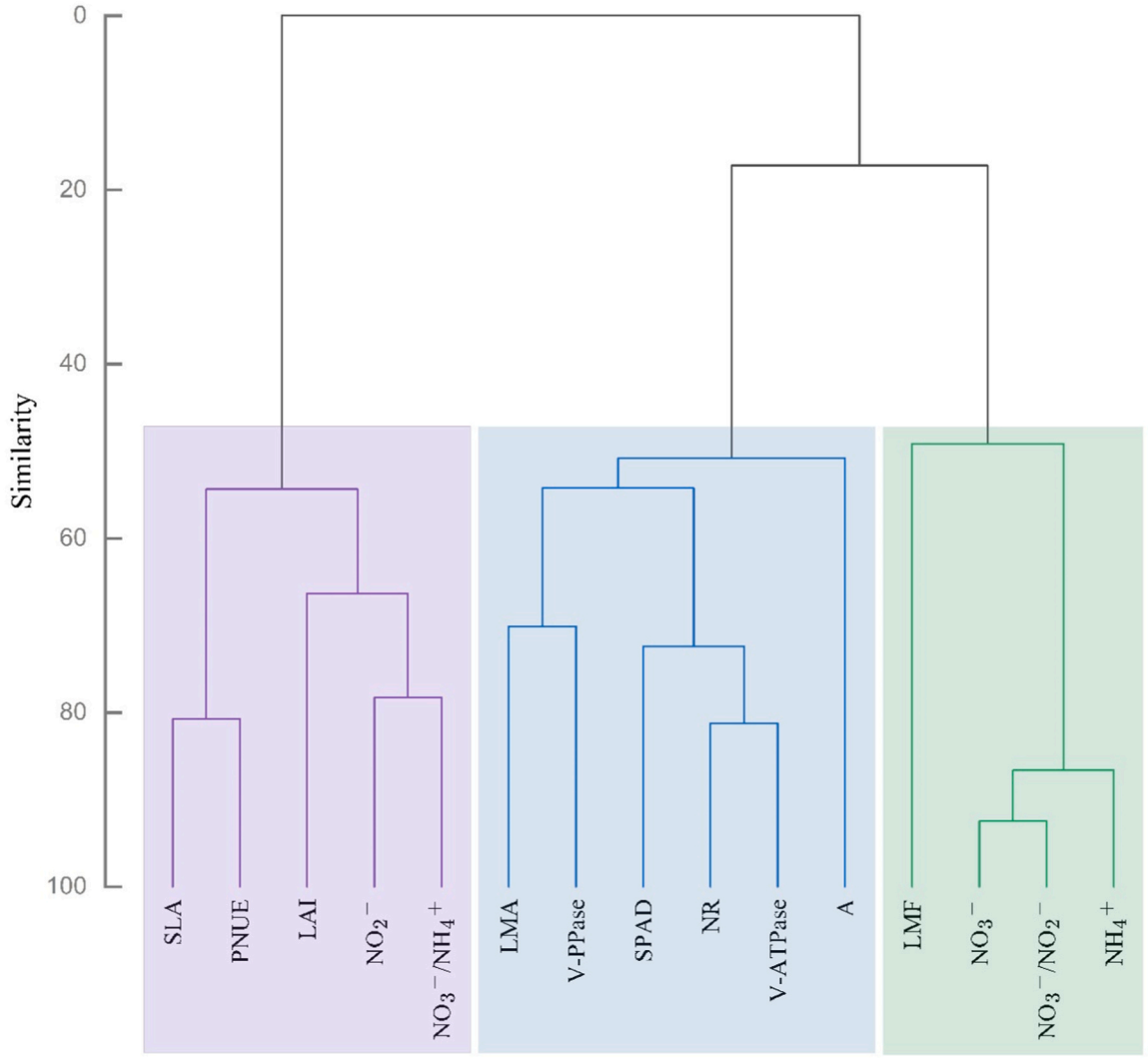

Fig. 8. Cluster analysis of selected traits related to leaf area dynamics, nitrogen assimilation and cellular energetics in A. rugosa under different light and nutrient levels. Abbreviations: SLA, specific leaf area; LMA, leaf mass area; LMF, leaf mass fraction; LAI, leaf area index; A, net photosynthesis rate; SPAD, relative chlorophyll content; NR, nitrate reductase; NO_3^-, nitrate; NO_2^-, nitrite; NH_4^+, ammonium; NO_3^-/NO_2^-, nitrate/nitrite ratio; NO_3^-/NH_4^+, nitrate/ammonium ratio; PNUE, photosynthetic nitrogen use efficiency; V-ATPase, vacuolar H^+-ATPase; V-PPase, vacuolar H^+-pyrophosphatase. The traits in the boxes indicate that they have high similarity and are aggregated. The three boxes represent the four groups of clustering analysis results. Different colors are only used to better distinguish the three groups.

components explain over 58 % of the total trait variance, with the SLA-PNUE-LAI relationship contributing significantly to Dim1. This quantitative assessment strengthens our understanding of the hierarchical importance of these traits in plant adaptation. The identification of distinct trait clusters through HCA at a similarity of >70 % suggests the existence of coordinated physiological modules that govern responses to environmental changes, indicating this may be a conserved adaptive strategy in plants.

Our HCA analysis demonstrates a close association between relative chlorophyll content (SPAD), nitrate reductase (NR), and V-ATPase activities. This cluster is further backed by their proximity in the upper right quadrant of the PCA biplot, indicating positive correlations. Our results show these traits are closely associated with high-light and moderate to high-nutrient levels (HL-NPK2 ~HL-NPK4), implying that *A. rugosa* optimizes these processes in energy-rich environments. The correlation between SPAD and NR is consistent with earlier reports that higher chlorophyll content corresponds with increased nitrogen assimilation (Garai and Tripathy, 2018; Evans and Clarke, 2019). However, the novel aspect of our findings is the clear association of V-ATPase with these photosynthetic and nitrogen metabolism parameters. The vector angles in our PCA biplot provide further quantitative support for these relationships, with acute angles between V-ATPase, SPAD, and NR vectors indicating strong positive correlations. The loading values of these traits on Dim1 and Dim2 suggest that their coordinated response explains approximately 45 % of the total variance in our dataset, highlighting the central role of this regulatory network in plant adaptive mechanism. V-ATPase is required for efficient nitrate storage (Krebs et al., 2010). Nitrate uptake or reduction affects cytoplasmic pH homeostasis (Espen 2004), suggesting an indirect role for V-ATPase in regulating NR. Vacuolar acidification seems to support high photosynthetic capacity and efficient nitrogen assimilation at high-light and high-nutrient levels. We posit that V-ATPase may function as a master regulator in optimizing plant performance under changing environmental conditions, a hypothesis that warrants further investigation.

5. Conclusion

This study reveals novel mechanistic insights into how *A. rugosa* orchestrates its physiological responses to varying light and nutrient conditions via interconnected regulatory networks. Beyond the potential role of V-ATPase as a master regulator, we uncovered several crucial adaptations: the tight association between specific leaf area,

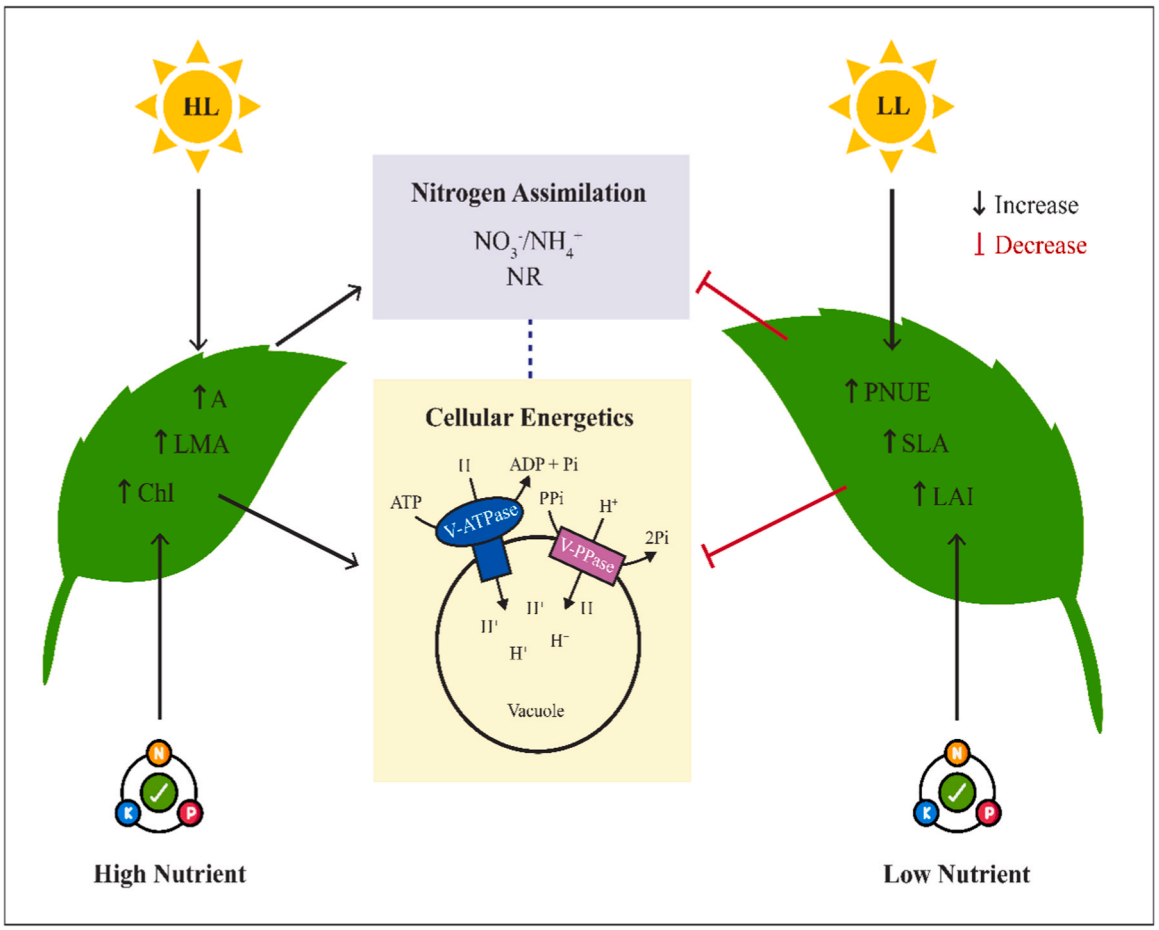

Fig. 9. Schematic diagram illustrating the changes in leaf dynamics, nitrogen assimilation, and cellular energetics in A. rugosa under different light and nutrient levels. Dashed line denotes potential interaction. Abbreviations: HL, high light; LL, low light; SLA, specific leaf area; LMA, leaf mass area; LAI, leaf area index; Chl, chlorophyll; A, net photosynthesis rate; NR, nitrate reductase; NO_3^-/NH_4^+, nitrate/ammonium ratio; PNUE, photosynthetic nitrogen use efficiency; ATP, adenosine triphosphate; ADP, adenosine diphosphate; Pi, inorganic phosphate; PPi, inorganic pyrophosphate; H^+, hydrogen ions; V-ATPase, vacuolar H^+-ATPase; V-PPase, vacuolar H^+-pyrophosphatase.

photosynthetic nitrogen use efficiency, and leaf area index in low-light but nutrient-rich environments; the synergistic enhancement of leaf mass area and nitrate reductase activity under high-light and nutrient conditions; and the maintenance of nitrogen homeostasis through balanced pools of different nitrogen forms. The clustering of leaf mass fraction with nitrogen-related traits and its distinctive downward vector in the PCA, suggests partially decoupled regulation of biomass allocation from other physiological processes - a finding that challenges the conventional view on resource allocation. The unexpected peak in proton pump activities under moderate nutrients and the strong correlation between chlorophyll content, nitrate reductase, and V-ATPase activity point to complex optimization strategies previously unreported in plant adaptation. Future study should focus on elucidating the molecular mechanisms governing these responses, particularly the signaling pathways linking V-ATPase activity to photosynthesis and nitrogen metabolism. Investigating whether these adaptive mechanisms are conserved across other species and their role in climate resilience can yield valuable insights for crop improvement. Meanwhile, the translational aspects of our findings, especially in developing stress-tolerant crops or optimizing cultivation practices for medicinal herbs like *A. rugosa*, represent promising areas for further investigation.

CRediT authorship contribution statement

Khairul Azree Rosli: Writing – review & editing, Writing – original draft, Visualization, Validation, Supervision, Software, Resources, Project administration, Methodology, Investigation, Funding acquisition, Formal analysis, Data curation, Conceptualization. **Azizah Misran:** Writing – review & editing, Supervision, Resources. **Latifah Saiful Yazan:** Writing – review & editing, Supervision. **Puteri Edaroyati Megat Wahab:** Writing – review & editing, Supervision, Resources, Funding acquisition, Conceptualization.

Declaration of Competing Interest

The authors declare that they have no known competing financial interests or personal relationships that could have appeared to influence the work reported in this paper.

Acknowledgements

This work has received funding from the Putra Graduate Initiative Grant (GP-IPS) from Universiti Putra Malaysia (Vot 9660900). We also acknowledge other researchers and staff for their excellent management and general skills.

Appendix A. Supporting information

Supplementary data associated with this article can be found in the online version at doi:10.1016/j.envexpbot.2024.106044.

Data availability

The data and materials supporting this study's findings are available from the corresponding author upon request.

References

Adavi, S.B., Sathee, L., Padhan, B.K., Singh, O., Meena, H.S., Durgesh, K., Jha, S.K., 2019. Visualization of nitric oxide, measurement of nitrosothiols content, activity of NOS and NR in wheat seedlings. Biol. Protoc. 9 (20), e3402. https://doi.org/10.21769/BioProtoc.3402.

Akhtar, K., Ain, N.ul, Prasad, P.V.V., Naz, M., Aslam, M.M., Djalovic, I., Riaz, M., Ahmad, S., Varshney, R.K., He, B., et al., 2024. Physiological, molecular, and environmental insights into plant nitrogen uptake, and metabolism under abiotic stresses. Plant Genome 17 (2), e20461. https://doi.org/10.1002/tpg2.20461.

An, J.H., Yuk, H.J., Kim, D.Y., Nho, C.W., Lee, D., Ryu, H.W., Oh, S.R., 2018. Evaluation of phytochemicals in *Agastache rugosa (Fisch. & C.A.Mey.) Kuntze* at different growth stages by UPLC-QTof-MS. Ind. Crops Prod. 112, 608–616.

Anand, S., Pang, E., Livanos, G., Mantri, N., 2018. Characterization of physico-chemical properties and antioxidant capacities of bioactive honey produced from Australian grown *Agastache rugosa* and its correlation with colour and poly-phenol content. Molecules 23 (1), 108.

Anten, N.P.R., During, H.J., 2011. Is analysing the nitrogen use at the plant canopy level a matter of choosing the right optimization criterion? Oecologia 167 (2), 293–303. https://doi.org/10.1007/s00442-011-2011-3.

Arnold, P.A., Kruuk, L.E.B., Nicotra, A.B., 2019. How to analyse plant phenotypic plasticity in response to a changing climate. N. Phytol. 222 (3), 1235–1241. https://doi.org/10.1111/nph.15656.

Bernacchi, C.J., Thompson, J.N., Coleman, J.S., Mcconnaughay, K.D.M., 2007. Allometric analysis reveals relatively little variation in nitrogen versus biomass accrual in four plant species exposed to varying light, nutrients, water and CO_2. Plant Cell Environ. 30 (10), 1216–1222. https://doi.org/10.1111/j.1365-3040.2007.01698.x.

Bernado, W.D., Baroni, D.F., Ruas, K.F., Santos, A.R., de Souza, S.B., Passos, L.C., Façanha, A.R., Ramalho, J.C., Campostrini, E., Rakocevic, M., et al., 2022. Ultraviolet radiation underlies metabolic energy reprograming in *Coffea arabica* and *Coffea canephora* genotypes. Sci. Hortic. 295, 110881. https://doi.org/10.1016/j.scienta.2022.110881.

Bowley, S., 1999. A hitchhiker's guide to statistics in plant biology. Guelph (ON). Any Old. Subj. Books.

Cisse, A., Zhao, X., Fu, W., Kim, R.E.R., Chen, T., Tao, L., Feng, B., 2020. Non-photochemical quenching involved in the regulation of photosynthesis of rice leaves under high nitrogen conditions. Int. J. Mol. Sci. 21 (6), 2115. https://doi.org/10.3390/ijms21062115.

Dietz, K.J., Tavakoli, N., Kluge, C., Mimura, T., Sharma, S.S., Harris, G.C., Chardonnens, A.N., Golldack, D., 2001. Significance of the V-type ATPase for the adaptation to stressful growth conditions and its regulation on the molecular and biochemical level. J. Exp. Bot. 52 (363), 1969–1980. https://doi.org/10.1093/jexbot/52.363.1969.

Esmaeili, S., Aliniaeifard, S., Dianati Daylami, S., Karimi, S., Shomali, A., Didaran, F., Telesiński, A., Sierka, E., Kalaji, H.M., 2022. Elevated light intensity compensates for nitrogen deficiency during chrysanthemum growth by improving water and nitrogen use efficiency. Sci. Rep. 12 (1), 10002. https://doi.org/10.1038/s41598-022-14163-4.

Evans, J.R., Clarke, V.C., 2019. The nitrogen cost of photosynthesis. J. Exp. Bot. 70 (1), 7–15. https://doi.org/10.1093/jxb/ery366.

Ezzine, M., Ghorbel, M.H., 2006. Physiological and biochemical responses resulting from nitrite accumulation in tomato (*Lycopersicon esculentum* Mill. cv. Ibiza F1). J. Plant Physiol. 163 (10), 1032–1039. https://doi.org/10.1016/j.jplph.2005.07.013.

Feng, Y.-L., Fu, G.-L., Zheng, Y.-L., 2008. Specific leaf area relates to the differences in leaf construction cost, photosynthesis, nitrogen allocation, and use efficiencies between invasive and noninvasive alien congeners. Planta 228 (3), 383–390. https://doi.org/10.1007/s00425-008-0732-2.

Figueroa, F., Israel, A., Neori, A., Martínez, B., Malta, E., Ang, P., Inken, S., Marquardt, R., Korbee, N., 2009. Effects of nutrient supply on photosynthesis and pigmentation in *Ulva lactuca* (Chlorophyta): responses to short-term stress. Aquat. Biol. 7, 173–183. https://doi.org/10.3354/ab00187.

Garai, S., Tripathy, B.C., 2018. Alleviation of nitrogen and sulfur deficiency and enhancement of photosynthesis in *Arabidopsis thaliana* by overexpression of uroporphyrinogen III methyltransferase (*UPM1*). Front. Plant Sci. 8. https://doi.org/10.3389/fpls.2017.02265. ⟨https://www.frontiersin.org/journals/plant-science/articles/10.3389/fpls.2017.02265/full⟩ [accessed 2024 Aug 22].

Gardner Z. 2019. Effects of fertilization and drying conditions on the quality of selected Chinese medicinal plants. [Amherst (MA)].

Gonçalves, J.F.D.C., Vieira, G., Marenco, R.A., Ferraz, J.B.S., Santos Junior, U.M.D., Barros, F.C.F., 2005. Nutritional status and specific leaf area of mahogany and tonka bean under two light environments. Acta Amaz. 35 (1), 23–27. https://doi.org/10.1590/S0044-59672005000100004.

Grassi, G., Colom, M.R., Minotta, G., 2001. Effects of nutrient supply on photosynthetic acclimation and photoinhibition of one-year-old foliage of *Picea abies*. Physiol. Plant. 111 (2), 245–254. https://doi.org/10.1034/j.1399-3054.2001.1110217.x.

Hachiya, T., Okamoto, Y., 2017. Simple spectroscopic determination of nitrate, nitrite, and ammonium in *Arabidopsis thaliana*. e2280–e2280 Biol. Protoc. 7 (10). https://doi.org/10.21769/BioProtoc.2280.

Haiyan, G., Lijuan, H., Shaoyu, L., Chen, Z., Ashraf, M.A., 2016. Antimicrobial, antibiofilm and antitumor activities of essential oil of *Agastache rugosa* from Xinjiang, China. Saudi J. Biol. Sci. 23 (4), 524–530. https://doi.org/10.1016/j.sjbs.2016.02.020.

Hikosaka, K., 2003. A model of dynamics of leaves and nitrogen in a plant canopy: An integration of canopy photosynthesis, leaf life span, and nitrogen use efficiency. Am. Nat. 162 (2), 149–164. https://doi.org/10.1086/376576.

Hikosaka, K., 2004. Leaf canopy as a dynamic system: Ecophysiology and optimality in leaf turnover. Ann. Bot. 95 (3), 521–533. https://doi.org/10.1093/aob/mci050.

Hikosaka, K., Yasumura, Y., Muller, O., Oguchi, R., 2014. Resource allocation and trade-offs in carbon gain of leaves under changing environment. In: Tausz, M., Grulke, N. (Eds.), Trees in a changing environment: Ecophysiology, adaptation, and future survival. Springer Netherlands, Dordrecht, pp. 1–24. https://doi.org/10.1007/978-94-017-9100-7_1.

Hou, H.D., Wu, C.Y., Zhou, J., Xu, J.D., Long, F., Zhu, J.H., Zhou, S.S., Zhang, W., Mao, Q., Shen, H., et al., 2022. Holistic quality evaluation of commercial *Agastache rugosa* by multiple chromatographic and chemometric analysis. J. Pharm. Biomed. Anal. 210, 114574. https://doi.org/10.1016/j.jpba.2021.114574.

Hunt R. 2012. Basic growth analysis: Plant growth analysis for beginners. London: Springer Science & Business Media.

Hyun Choong, O., Ji Sook, S., Yong Am, C., 2000. Effect of forms and levels of nitrogen fertilizer on plant growth and essential oil content of *Agastache rugosa*. Korean J. Crop Sci. 45 (2), 128–133.

Kiba, T., Krapp, A., 2016. Plant nitrogen acquisition under low availability: Regulation of uptake and root architecture. Plant Cell Physiol. 57 (4), 707–714. https://doi.org/10.1093/pcp/pcw052.

Kim, S.W., 2020. Korean native wild herbal-based functional ingredient for skin health: Agatri® (*Agastache rugosa* extract). Food Sci. Ind. 53 (4), 382–389.

Kim S.J., Park J.E., Bok G.J., Kanth B.K., Lam V.P., Park J.S. 2018. High electrical conductivity of nutrient solution and application of methyl jasmonate promote phenylpropanoid production in hydroponically grown Agastache rugosa. 원예과학기술지. 36(6):841–852. doi:10.12972/kjhst.20180082.

Kitajima, K., Wright, S.J., Westbrook, J.W., 2016. Leaf cellulose density as the key determinant of inter- and intra-specific variation in leaf fracture toughness in a species-rich tropical forest. Interface Focus 6 (3), 20150100. https://doi.org/10.1098/rsfs.2015.0100.

Klodd, A., Nippert, J., Ratajczak, Z., Waring, H., Phoenix, G., 2016. Tight coupling of leaf area index to canopy nitrogen and phosphorus across heterogeneous tallgrass prairie communities. Oecologia 182, 889–898. https://doi.org/10.1007/s00442-016-3713-3.

Koistinen, J., Sjöblom, M., Spilling, K., 2019. Total nitrogen determination by a spectrophotometric method. In: Biofuels from algae: Methods and protocols. Springer, New York, NY, pp. 81–86.

Krapp, A., 2015. Plant nitrogen assimilation and its regulation: a complex puzzle with missing pieces. Curr. Opin. Plant Biol. 25, 115–122. https://doi.org/10.1016/j.pbi.2015.05.010.

Kriegel, A., Andrés, Z., Medzihradszky, A., Krüger, F., Scholl, S., Delang, S., Patir-Nebioglu, M.G., Gute, G., Yang, H., Murphy, A.S., et al., 2015. Job sharing in the endomembrane system: Vacuolar acidification requires the combined activity of V-ATPase and V-PPase. Plant Cell 27 (12), 3383–3396. https://doi.org/10.1105/tpc.15.00733.

Kumari, Ankita, Sharma, H., Kumari, Archana, Sharma, P., Pathak, N., Singh, R., Al-Tawaha, A.R., Pandey, D.K., Shekhawat, M.S., Mandal, S., 2024. Movement and signaling of macronutrients in plant system. In: Plant biology, sustainability and climate change. Elsevier, pp. 1–28. https://doi.org/10.1016/B978-0-443-16082-0.00005-9.

Lee, Y., Lim, H.-W., Ryu, I.W., Huang, Y.-H., Park, M., Chi, Y.M., Lim, C.-J., 2020. Anti-inflammatory, barrier-protective, and antiwrinkle properties of *Agastache rugosa* Kuntze in human epidermal keratinocytes. BioMed. Res. Int. 2020, e1759067. https://doi.org/10.1155/2020/1759067.

Li, L., Liu, K.-H., Sheen, J., 2021. Dynamic nutrient signaling networks in plants. Annu. Rev. Cell Dev. Biol. 37, 341–367. https://doi.org/10.1146/annurev-cellbio-010521-015047.

Lillo, C., 2004. Light regulation of nitrate uptake, assimilation and metabolism. In: Amâncio, S., Stulen, I. (Eds.), Nitrogen acquisition and assimilation in higher plants. Springer Netherlands, Dordrecht, pp. 149–184. https://doi.org/10.1007/978-1-4020-2728-4_6.

Liu, S., He, F., Kuzyakov, Y., Xiao, H., Hoang, D.T.T., Pu, S., Razavi, B.S., 2022. Nutrients in the rhizosphere: a meta-analysis of content, availability, and influencing factors. Sci. Total Environ. 826, 153908. https://doi.org/10.1016/j.scitotenv.2022.153908.

Lu, Z., Ren, T., Li, J., Hu, W., Zhang, J., Yan, J., Li, X., Cong, R., Guo, S., Lu, J., 2020. Nutrition-mediated cell and tissue-level anatomy triggers the covariation of leaf photosynthesis and leaf mass per area. In: Raines, C. (Ed.), Journal of Experimental Botany, 71, pp. 6524–6537. https://doi.org/10.1093/jxb/eraa356.

Maeshima, M., 2001. Tonoplast transporters: organization and function. Annu. Rev. Plant Biol. 52 (52, 2001), 469–497. https://doi.org/10.1146/annurev.arplant.52.1.469.

Moore, K.J., Dixon, P.M., 2015. Analysis of combined experiments revisited. Agron. J. 107 (2), 763–771. https://doi.org/10.2134/agronj13.0485.

Motsara, M.R., Roy, R.N., 2008. Guide to laboratory establishment for plant nutrient analysis. FAO, Rome.

Park, W.T., Yeo, S.K., Sathasivam, R., Park, J.S., Kim, J.K., Park, S.U., 2020. Influence of light-emitting diodes on phenylpropanoid biosynthetic gene expression and phenylpropanoid accumulation in *Agastache rugosa*. Appl. Biol. Chem. 63, 1–9. https://doi.org/10.1186/s13765-020-00510-4.

Parker, G.G., 2020. Tamm review: leaf area index (LAI) is both a determinant and a consequence of important processes in vegetation canopies. For. Ecol. Manag. 477, 118496. https://doi.org/10.1016/j.foreco.2020.118496.

Pashkovskiy, P., Kreslavski, V., Khudyakova, A., Ashikhmin, A., Bolshakov, M., Kozhevnikova, A., Kosobryukhov, A., Kuznetsov, V.V., Allakhverdiev, S.I., 2021. Effect of high-intensity light on the photosynthetic activity, pigment content and expression of light-dependent genes of photomorphogenetic *Solanum lycopersicum hp* mutants. Plant Physiol. Biochem. 167, 91–100. https://doi.org/10.1016/j.plaphy.2021.07.033.

Pearcy, R.W., Muraoka, H., Valladares, F., 2005. Crown architecture in sun and shade environments: assessing function and trade-offs with a three-dimensional simulation model. N. Phytol. 166 (3), 791–800. https://doi.org/10.1111/j.1469-8137.2005.01328.x.

Poorter, H., Niinemets, Ü., Ntagkas, N., Siebenkäs, A., Mäenpää, M., Matsubara, S., Pons, ThijsL., 2019. A meta-analysis of plant responses to light intensity for 70 traits ranging from molecules to whole plant performance. N. Phytol. 223 (3), 1073–1105. https://doi.org/10.1111/nph.15754.

Poorter, H., Niinemets, Ü., Poorter, L., Wright, I.J., Villar, R., 2009. Causes and consequences of variation in leaf mass per area (LMA): a meta-analysis. N. Phytol. 182 (3), 565–588. https://doi.org/10.1111/j.1469-8137.2009.02830.x.

Qiang, B., Zhou, W., Zhong, X., Fu, C., Cao, L., Zhang, Y., Jin, X., 2023. Effect of nitrogen application levels on photosynthetic nitrogen distribution and use efficiency in soybean seedling leaves. J. Plant Physiol. 287, 154051. https://doi.org/10.1016/j.jplph.2023.154051.

Quebbeman, J.A., Ramirez, J.A., 2016. Optimal allocation of leaf-level nitrogen: Implications for covariation of cmax and max and photosynthetic downregulation. J. Geophys. Res. Biogeosci. 121 (9), 2464–2475. https://doi.org/10.1002/2016JG003473.

Röver, A., Koch, H.J., 1995. Indirect determination of leaf area index of sugar beet canopies in comparison to direct measurement. J. Agron. Crop Sci. 174 (3), 189–195. https://doi.org/10.1111/j.1439-037X.1995.tb01102.x.

Sakuraba, Y., Yanagisawa, S., 2018. Light signalling-induced regulation of nutrient acquisition and utilisation in plants. Semin. Cell Dev. Biol. 83, 123–132. https://doi.org/10.1016/j.semcdb.2017.12.014.

Schieving, F., Poorter, H., 1999. Carbon gain in a multispecies canopy: the role of specific leaf area and photosynthetic nitrogen-use efficiency in the tragedy of the commons. N. Phytol. 143 (1), 201–211. https://doi.org/10.1046/j.1469-8137.1999.00431.x.

Segami, S., Asaoka, M., Kinoshita, S., Fukuda, M., Nakanishi, Y., Maeshima, M., 2018. Biochemical, structural and physiological characteristics of vacuolar H^+-pyrophosphatase. Plant Cell Physiol. 59 (7), 1300–1308. https://doi.org/10.1093/pcp/pcy054.

Shah, I.H., Jinhui, W., Li, X., Hameed, M.K., Manzoor, M.A., Li, P., Zhang, Y., Niu, Q., Chang, L., 2024. Exploring the role of nitrogen and potassium in photosynthesis implications for sugar: accumulation and translocation in horticultural crops. Sci. Hortic. 327, 112832. https://doi.org/10.1016/j.scienta.2023.112832.

Singh R., Mahajan J., Arora S., Bhardwaj R., Kaur T.. 2021. Physiological role of mineral nutrients and their uptake during abiotic stress. In: Kaur T, Arora S, editors. Bentham Science Publishers. p. 75–88. https://www.eurekaselect.com/node/193092.

Tegeder, M., Masclaux-Daubresse, C., 2018. Source and sink mechanisms of nitrogen transport and use. New Phytol. 217 (1), 35–53. https://doi.org/10.1111/nph.14876.

Vargas, M., Glaz, B., Alvarado, G., Pietragalla, J., Morgounov, A., Zelenskiy, Y., Crossa, J., 2015. Analysis and interpretation of interactions in agricultural research. Agron. J. 107 (2), 748–762. https://doi.org/10.2134/agronj13.0405.

Vega-Mas, I., Sarasketa, A., Marino, D., 2015. High-throughput quantification of ammonium content in Arabidopsis. Biol. Protoc. 5 (16), 14–17. https://doi.org/10.21769/BioProtoc.1559.

Wicharuck, S., Suang, S., Chaichana, C., Chromkaew, Y., Mawan, N., Soilueang, P., Khongdee, N., 2024. The implementation of the SPAD-502 Chlorophyll meter for the quantification of nitrogen content in Arabica coffee leaves. MethodsX 12, 102566. https://doi.org/10.1016/j.mex.2024.102566.

Wu, Y., Shi, L., Li, L., Fu, L., Liu, Y., Xiong, Y., Sheen, J., 2019. Integration of nutrient, energy, light, and hormone signalling via TOR in plants. J. Exp. Bot. 70 (8), 2227–2238. https://doi.org/10.1093/jxb/erz028.

Xu, G., Fan, X., Miller, A.J., 2012. Plant nitrogen assimilation and use efficiency. Annu. Rev. Plant Biol. 63, 153–182. https://doi.org/10.1146/annurev-arplant-042811-105532.

Yamani, H., Mantri, N., Morrison, P.D., Pang, E., 2014. Analysis of the volatile organic compounds from leaves, flower spikes, and nectar of Australian grown *Agastache rugosa*. BMC Complement. Altern. Med. 14 (1), 495. https://doi.org/10.1186/1472-6882-14-495.

Ye, M., Peng, S.B., Li, Y., 2019. Intraspecific variation in photosynthetic nitrogen-use efficiency is positively related to photosynthetic rate in rice (*Oryza sativa* L.) plants. Photosynthetica 57 (1), 311–319. https://doi.org/10.32615/ps.2019.011.